THE JOURNAL OF PHYSICAL CHEMISTRY C

Article

Cite This: J. Phys. Chem. C 2018, 122, 24891−24895

pubs.acs.org/JPCC

Imaging Nanoscale Heterogeneity in Ultrathin Biomimetic and Biological Crystals

Brian T. O'Callahan,[†] Kevin T. Crampton,[‡] Irina V. Novikova,[†] Tengyue Jian,[‡] Chun-Long Chen,[‡] James E. Evans,[†,⊥] Markus B. Raschke,[§] Patrick Z. El-Khoury,[‡] and A. Scott Lea*[,†]

[†]Environmental and Molecular Sciences Laboratory and [‡]Physical Sciences Division, Pacific Northwest National Laboratory, Richland, Washington 99352, United States

[§]Department of Physics, Department of Chemistry, and JILA, University of Colorado at Boulder, Boulder, Colorado 80309, United States

[⊥]School of Biological Sciences, Washington State University, Pullman, Washington 99164, United States

Supporting Information

ABSTRACT: The mechanisms of interface biochemistry are often obscured through ensemble averaging of complex networks of proteins that exhibit varying degrees of structural heterogeneity. Here, we perform nanometer spatially resolved chemical spectroscopy using infrared vibrational scattering-scanning near-field optical microscopy (IR *s*-SNOM) to image protein−protein interactions and conformational heterogeneity of (i) a two-dimensional lipid-like peptoid membrane and (ii) a three-dimensional catalase crystal. In the peptoid membrane, which consists of stacked ∼4 nm high peptoid layers, spatio-spectral line width analyses reveal heterogeneity of the vibrational dynamics due to peptoid−substrate and peptoid−peptoid interactions. In *s*-SNOM imaging of catalase crystals, our results revealed complex secondary structures that vary over nanometer length scales. Broadening of vibrational resonances, as observed from the dehydrated catalase crystals, indicates a higher degree of heterogeneity as compared to the synthetic peptoid membranes. Our results thus demonstrate the utility of IR nanoscopy for the investigation of structural heterogeneity within biomimetic and biological systems with high spatio-spectral resolution and sensitivity.

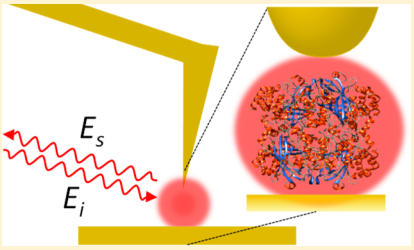

INTRODUCTION

Biomolecular systems and low-dimensional cellular constructs, e.g., membranes and protein complexes, may be regarded as the architectures that cooperatively sustain interface biochemistry. The functional properties of such systems are derived from protein−protein interactions at the molecular level, which, in turn, govern the formation of secondary structures.[1] While the latter are increasingly well-characterized at the ensemble level,[2−4] understanding the nanoscopic, protein-level interactions that translate into long-range order, or lack thereof, remains an outstanding challenge. Our chemical understanding of biointerfaces thus hinges on the advancement of imaging modalities with high sensitivity to intermolecular coupling and disorder over the nanometer length scales of relevance to biological systems.

Of the various approaches to chemical nanoimaging, infrared or Raman vibrational near-field optical microscopy and spectroscopy, enabled through nanoconfined optical fields, are particularly attractive due to their ability to simultaneously provide chemical specificity and nanoscale resolution. Scattering-based scanning near-field optical microscopy (*s*-SNOM) utilizing near- to mid-infrared (IR) radiation is of particular interest for biological and biomimetic applications, as has been exploited recently to demonstrate nanoscale (<30 nm) vibrational imaging of secondary structure in amyloid fibrils,[5] membrane proteins in bacteriorhodopsin,[6] single-stranded RNA viruses,[7] and peptoid nanosheets.[8] Given the inherent sensitivity of IR spectroscopy to long-range material symmetry, IR *s*-SNOM provides an efficient route to conduct conformational analyses in the near-field,[9] e.g., through the amide bands of common proteins.[10] Such conformational selectivity is a prerequisite for characterizing nanometric structure in bio-relevant crystalline materials.

Quite generally, fundamental information about both the ultrafast processes that govern molecule-environment coupling and the inherent material spatial and structural heterogeneity is embedded in the vibrational line widths accessible with spectroscopic *s*-SNOM. In this context, local variations in vibrational frequencies and lifetimes have revealed variability in sample crystallinity,[11] intermolecular coupling,[12] and tip- or substrate-mediated antenna coupling.[13] Despite the foregoing demonstrations that have highlighted the utility of *s*-SNOM, few studies have applied spectral line width analysis to near-field spectroscopy for a more detailed understanding of order and local interactions in a wider range of biomolecular systems.

Received: July 12, 2018
Revised: August 31, 2018
Published: September 25, 2018

DOI: 10.1021/acs.jpcc.8b06681
J. Phys. Chem. C 2018, 122, 24891−24895

Here, we describe correlated atomic force microscopy (AFM) and IR *s*-SNOM imaging of a peptoid-based 2D membrane-mimetic nanomaterial (peptoid sheet) and a 3D ultrathin catalase crystal. These measurements utilize the joint high spatial and spectral sensitivity of IR *s*-SNOM to reveal nanoscopic details of biomolecular order and local molecular interactions. We observe heterogeneous distributions of vibrational line widths and amplitudes, varying over tens of nm, that ultimately discriminate mono- versus multilayer peptoid−substrate and peptoid−peptoid interactions in the peptoid crystal and long-range secondary structure in the catalase crystal. By providing spectroscopic information with nanoscale spatial resolution, these results demonstrate the IR *s*-SNOM can provide insight into the local organization of secondary structures in 2D and 3D protein systems that underlies their biological function.

EXPERIMENTAL METHODS

AFM and IR *s*-SNOM. We performed scattering-scanning near-field optical microscopy (*s*-SNOM) by focusing IR light onto the sharp apex of a gold-coated scanning probe tip of an atomic force microscope (attoAFM II, Attocube) operating in tapping mode as described previously.[6,9] A quantum cascade laser (MIRcat, Daylight Solutions) provided monochromatic light tunable across the amide region from 1530 to 1740 cm^{-1}. The spectral resolution is nominally limited by the laser frequency step size of 0.5 cm^{-1}. Scattered light, which is produced when the tip is brought in proximity to the sample, reflects the local vibrational properties of the sample within a focal volume dictated by the tip apex radius (∼20 nm). The tip-scattered light was combined with light from a reference arm split from the source laser and is detected with a mercury−cadmium−telluride detector. Lock-in demodulation was performed at the third harmonic of the cantilever oscillation frequency to suppress the terms independent of the tip-scattered near-field signal, E_{nf}. In this limit, the intensity at the detector reduces to

$$I \approx 2Re(E_{nf}^{*}E_{ref}) + 2Re(E_{nf}^{*}E_{bkg})$$

where E_{ref} and E_{bkg} are the electric fields of the reference arm and the background, respectively. The latter is a result of scattering and reflection within the diffraction-limited focal spot. The near-field phase, providing an easily interpretable signal for vibrational resonances, was extracted using two-phase homodyne in which images are captured at two reference arm positions shifted by $\Delta\phi = \pi/4 = \lambda/8$.[14] We isolated the second term in the above expression, which is due to spurious backgrounds, by acquiring an additional image with the reference arm blocked. We then subtracted the resulting image from the measured signal with the reference arm unblocked. Note, the presented phase images represent an average of 4−5 individual acquisitions under the noted frequency window(s). To estimate the spatial resolution of our optical images, we apply exponential fits to the line profiles and assign the $1/e$ signal rise length Δx, as the lateral resolution of the vibrational response.

Sample Preparation. The 2D peptoid sheets were assembled from amphiphilic, lipid-like peptoids containing two sub-blocks, respectively, six polar residues, *N*-(2-carboxyethyl)glycine (Nce), and six nonpolar residues, *N*-[2-(4-chlorophenyl)ethyl]glycines (N4-Clpe)[15] (see Supporting Information for additional details) and were drop-cast onto a freshly cleaved template-stripped gold substrate (Au.1000.SWTSG, Platypus Technologies) that was used with no additional cleaning. The Au surface provides IR signal enhancement due to tip−sample polarization enhancement.[16] A terraced region of the peptoid crystal, which dries upon mounting, was selected to investigate the thickness dependence of the crystal nanospectroscopic properties. The 3D catalase crystals were prepared according to previously published protocol.[17] In short, 240 μL of aqueous suspension of catalase from bovine liver (C100, Sigma) were centrifuged at 5 000*g* for 2 min. The supernatant was removed, and the pellet was resuspended in 480 μL of water. The centrifugation step was repeated, and the pellet was washed with the same amount of water once more. Then the pellet was further solubilized in 240 μL of 1.7 M NaCl, mixed over 5 min period, and centrifuged at 16 000*g* for 10 min. The supernatant, which contained the soluble catalase, was dialyzed overnight at 4 °C against 50 mM sodium phosphate buffer (pH 6.3). The solution was then transferred to a new test tube and left at 4 °C for several days until a visible precipitate formed. Well-ordered catalase crystal formation was confirmed by cryo-transmission electron microscopy (cryo-TEM) (diffraction observed at 3 Å; see Supporting Information Figure S1) using conventional methods for sample vitrification on a Leica EM GP instrument and cryo-TEM and electron diffraction on a FEI Titan environmental-TEM instrument. For *s*-SNOM experiments, 2 μL of suspension of catalase crystals were drop-cast on a gold substrate and allowed to air-dry.

RESULTS AND DISCUSSION

The biomimetic and biomolecular systems studied herein are illustrated in Figure 1. The 2D peptoid sheet, shown in Figure 1a, is composed of a bilayer-like packing of 12-mer peptoids arranged in a highly crystalline structure of ∼4 nm thickness.[15] The catalase protein tetramer, which is the base unit for the 3D catalase crystals, is displayed in Figure 1b, with the α-helix and the β-sheet secondary structures highlighted in red and blue, respectively. In both systems, we selectively target the amide I vibrational resonance, which serves as a sensitive probe of protein secondary structure.[10]

Figure 2 shows the results of correlated AFM and *s*-SNOM imaging and spectroscopy recorded on peptoid sheet(s) within the IR amide-I region spanning 1644 to 1686 cm^{-1}, acquired at 1−2 cm^{-1} frequency steps. A detailed description of the scanning probe apparatus and sample preparation information are given in the Experimental Methods section. Briefly, the system consisted of highly ordered peptoid nanosheets prepared on a template-stripped gold substrate. The underlying gold substrate was utilized in conjunction with a gold-coated AFM probe tip to provide high field enhancement and confinement to enhance the *s*-SNOM molecular response, which we recorded interferometrically through a single-reference demodulation scheme.[14] The resulting near-field spectral phase then carries the local molecular vibrational information, which mimics the IR absorption spectrum (see Experimental Methods). The AFM topography, shown in Figure 2a, reveals distinct spatial regions corresponding to the bare gold substrate, the peptoid ML, and folded or terraced peptoid layers. A corresponding *s*-SNOM phase image-averaged over five acquisitions at different frequencies, ν = 1660, 1661.5, 1662, 1663, and 1665.5 cm^{-1}, is shown in Figure 2b, with the IR signature of the C═O stretch of the repeated amide groups primarily providing the peptoid contrast observed.[7,10] Cross sections of the phase image acquired across the gold−peptoid boundary and peptoid ML−

DOI: 10.1021/acs.jpcc.8b06681
J. Phys. Chem. C 2018, 122, 24891−24895

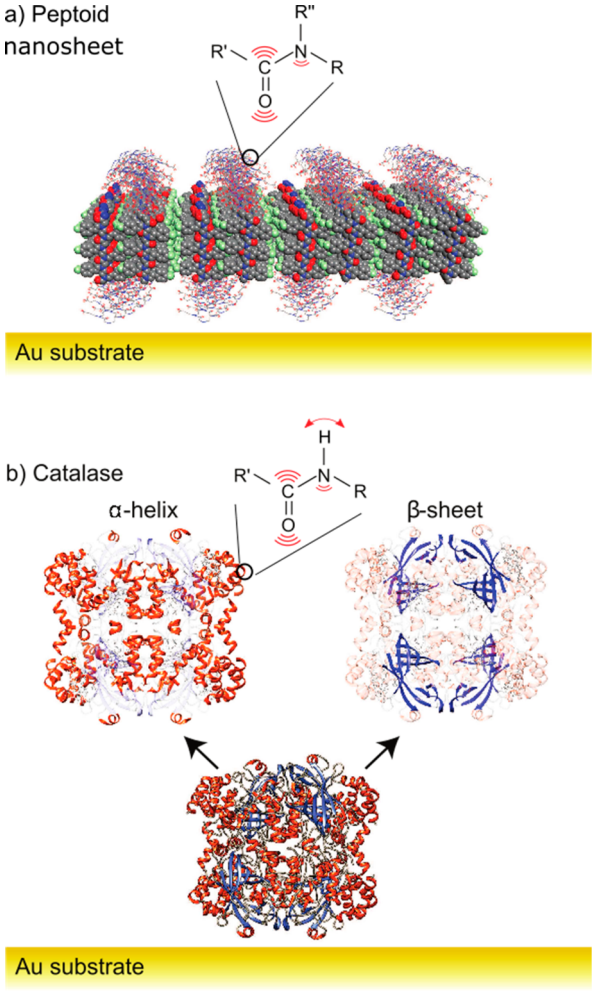

Figure 1. Illustrations of (a) 2D peptoid nanosheet consisting of repeated amide chains in highly crystalline structure and (b) single catalase tetramer, consisting of a mixture of α-helix (red) and β-sheet (blue) moieties. Both systems were prepared on nearly atomically smooth, template-stripped gold substrates.

BL terrace are shown as solid lines in Figure 2c, with corresponding exponential fits as dashed lines. The measured lateral resolution of the vibrational response is $\Delta x \approx 20$ nm, as described in the Experimental Methods, directly reflecting the radius of the scanning tip apex[18] of typically ~20 nm. Using the peptoid spacing of 4.5 Å and 1.8 nm in the *X*- and *Y*-directions, respectively, as determined by X-ray diffraction,[15] we estimate that the focal volume in these measurements targets $\sim 10^3$ individual peptoids and correspondingly $\sim 10^3$–10^4 individual amide groups. Moreover, based on the demonstrated signal-to-noise ratio of ~20:1, we estimate that a lower sensitivity limit of as small as ~100 peptoids may be obtained with a signal-to-noise of 1:1.

We further characterized the observed vibrational response by recording phase images at discrete laser frequencies in the vicinity of ~1662 cm^{-1}, for a total set of 20 images. This allowed individual IR spectra to be recorded at every image pixel within the field of view. Extracted representative spectra, acquired at points corresponding to the ML, BL, and TL positions as indicated in Figure 2a and b, are shown in Figure 2d. The vibrational profiles fit well to Lorentzian lineshapes of fwhm $\Delta\nu$ = 8.5 cm^{-1} centered at ν = 1663 cm^{-1} (Figure 2d solid lines) and

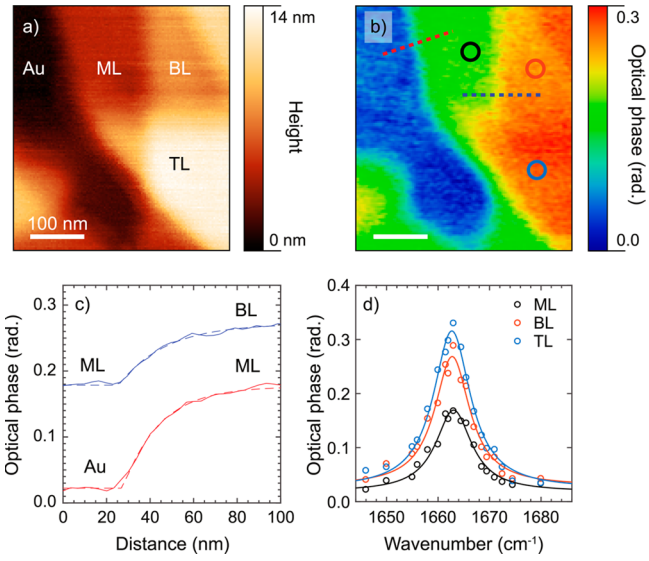

Figure 2. Correlated AFM and IR *s*-SNOM imaging and spectroscopy recorded on the peptoid sheet(s). (a) AFM topography revealing monolayer (ML), bilayer (BL), and trilayer (TL) regions. (b) *s*-SNOM phase image recorded on-resonance at ν = 1662 cm^{-1}, and (c) optical phase cross sections of the stacked layers (solid lines) acquired where indicated in (b), along with exponential fits (dashed lines). Each layer has a thickness of ~4 nm. (d) Point spectra (open circles) and Lorentzian fits (solid lines) recorded at the ML, BL, and TL positions as indicated in (b).

are consistent with the amide I resonance for α-helical structured protein as noted above.

The extracted line widths, $\Delta\nu$, exhibit considerable heterogeneity across the probed region. We explored this quantitatively through a spatio-spectral analysis of the peptoid *s*-SNOM results, as summarized in Figure 3. This analysis utilized 15 × 15 nm subregions of the larger phase map through which we performed a moving average Lorentzian fit of the entire data set. A spatial map of the extracted line widths is shown in Figure 3a. The observed variation in $\Delta\nu$ of 4–12 cm^{-1} loosely tracks the ML, BL, and TL regions of the peptoid. Figure 3b shows the corresponding line width statistics extracted from averaged sections of each layer as histograms. As can be seen, as the layer thickness increased from ML to TL, the variance in $\Delta\nu$ converges to as narrow as ~1 cm^{-1}. The extracted heterogeneity in $\Delta\nu$ represents spatial variation in the degree of order and crystallinity,[19,20] with higher, most likely substrate-induced disorder for the ML,[21] compared to well-ordered BL and TL regions that are stabilized by attractive van der Waals forces. Figure 3c shows a spatial map of the peak frequency, with corresponding histograms in Figure 3d, which illustrates a gradual red-shift of the resonance frequency as the layer number increases. As observed previously in *s*-SNOM studies of polymers, bond softening occurs when a vibrational mode is subject to a solvent field resulting in a spectral red-shift.[12] We thus attribute the red-shift on the BL and the TL regions to a solvatochromatic shift due to electrostatic interactions between the densely packed amide groups of the stacked peptoid layers.[22] While image-dipole coupling of the amide vibrational modes and the Au substrate and probe tip can modify vibrational lifetimes and vibrational frequencies,[13] we do not expect this to be significant due to the high localization of the vibrational modes and their relatively large average distance from Au substrate.

DOI: 10.1021/acs.jpcc.8b06681
J. Phys. Chem. C 2018, 122, 24891–24895

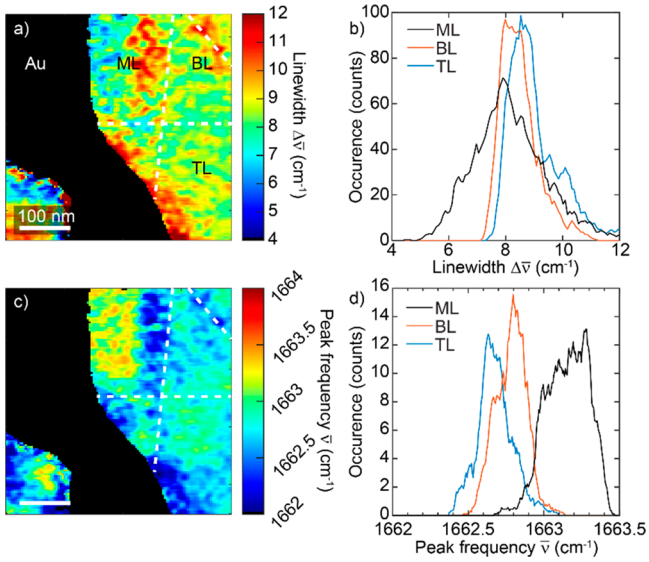

Figure 3. Spatio-spectral analysis of the peptoid *s*-SNOM results presented in Figure 2. (a) Spatial map and (b) histogram of spectral line width generated through Lorentzian fits of each pixel. Scale bar is 100 nm. White dashed lines indicate boundaries between ML, BL, and TL regions. (c) Corresponding spatial map and (d) histogram of the peak position. The ML region is characterized by a slight shift in peak frequency and more pronounced heterogeneity in the spectral line width compared to the BL and TL regions.

We then performed similar measurements targeting the three-dimensional catalase crystal, which is also drop-cast on a gold substrate. The catalase, derived from bovine liver, represents a model protein system with complex secondary and tertiary structures that provides an excellent platform to test the vibrational sensitivity of *s*-SNOM on the tens of nm length scale. The results are summarized in Figure 4, and details of the catalase crystal growth may be found in the Experimental Methods section. The AFM topography (Figure 4a) exhibits crystal height variations ranging from ~20 to 35 nm. In contrast to the peptoid sheet(s), the vibrational response of the catalase crystal is broad as a result of contributions from multiple vibrational bands that are indicative of a mixture of secondary structures. This is evidenced by point spectra (Figure 4b) acquired at the positions indicated in Figure 4a, which span ~50 cm^{-1} in spectral width with ~5 cm^{-1} frequency steps. Phase images spectrally integrated over frequencies ν = 1650, 1655, 1665, 1670, and 1676 cm^{-1} and 1620, 1625, 1630, and 1635 cm^{-1} are shown in Figure 4c and d, respectively. The spectrally disparate phase maps exhibit corrugation on the tens of nm length scale that is seemingly uncorrelated to the overall AFM topography.

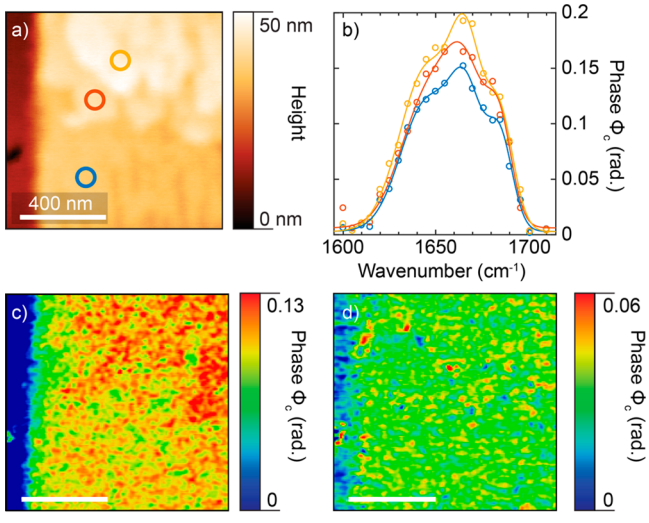

Figure 4. Correlated AFM and *s*-SNOM images recorded on a three-dimensional catalase crystal. (a) AFM topography of the crystal and the underlying gold substrate. Over the interrogated region, the crystal thickness varies from ~20 to 35 nm. (b) Point spectra (open circles) recorded at the locations indicated in (a) along with Gaussian fits (solid lines, see text). Phase images acquired in the spectral ranges from 1650 to 1676 cm^{-1} and 1620–1635 cm^{-1} are shown in (c) and (d), respectively.

We fit the spectra to the sum of three Gaussian lineshapes through a least-squares procedure to evaluate the secondary structure and its nanoscale variation within the crystallite. We find that the measured features are well-represented by individual vibrational peaks centered at ν_1 = 1643, ν_2 = 1666, and ν_3 = 1684 cm^{-1} with corresponding line widths ranging from 16 to 32 cm^{-1} (tabulated fit parameters are given in the Supporting Information Table S1). On the basis of the peak frequencies associated with the fitting, we assign the bright feature at ν_2 = 1666 cm^{-1} to the α-helix amide I mode and the remaining features, which flank the amide I peak, to the β-sheet at ν_1 = 1643 cm^{-1} and the random coil moiety at ν_3 = 1684 cm^{-1}. This distribution of secondary structures agrees with the known vibrational signatures of protein secondary structures[10] known to be present in catalase 3D crystals.[23]

The ~10 nm surface corrugations observed in the AFM topography and the inhomogeneous nature of the IR spectra reflect a high degree of local heterogeneity within the catalase crystal. Compared to the peptoid imaging results, these measurements effectively demonstrate nanoscale vibrational imaging of disorder in a protein crystal. While cryo-TEM confirmed a high degree of crystallinity for the catalase sample when fully hydrated, the drying process prior to *s*-SNOM imaging (due to the drop-casting method used for these measurements) may have introduced the disorder in the crystal observed via loss of stabilizing hydration shells. While our current system is limited to ambient analyses, the observed heterogeneity motivates in situ nanoscopy targeting the hydrated form(s) of the systems studied herein. In the absence of long-range material symmetry, the factors governing the preferential localization of secondary structures, as observed here, are complex in biological systems at the nanoscale, especially under dehydrated and ambient conditions.

CONCLUSION

In summary, we have demonstrated correlated AFM and IR *s*-SNOM imaging measurements on 2D peptoid sheet(s) and a 3D catalase crystal. We obtain 20 nm lateral spatial resolution with monolayer sensitivity of the highly ordered peptoid system through near-field vibrational imaging via the amide I band. This allowed us to spectroscopically discriminate individual peptoid layers in folded or terraced regions of this system. Nanoscale heterogeneity in the spectral line width is prominent at the ML level, likely induced by substrate morphology. Alternatively, the observed resonance frequency variations primarily arise as a result of chemical interactions between the layers, highlighting the utility of IR *s*-SNOM as a robust probe that is capable of disentangling protein–protein and protein–substrate interactions. These observations also suggest that functional properties

DOI: 10.1021/acs.jpcc.8b06681
J. Phys. Chem. C 2018, 122, 24891–24895

governed by protein chemistry in biomimetic systems may be tailored through substrate modification. In contrast, we extracted inhomogeneously broadened spectral features from dehydrated catalase protein crystals that reflect a higher degree of heterogeneity with nanoscale spectral signatures, indicating a mixture of secondary structures, which we assign herein above. Our results thus demonstrate the ability of IR *s*-SNOM to identify the spectral signatures of order/disorder in biological systems with nanoscale precision and motivate further development and extension into in situ and in-liquid conditions to reveal the mechanisms underlying function in live biological systems.

■ ASSOCIATED CONTENT

Supporting Information

The Supporting Information is available free of charge on the ACS Publications website at DOI: 10.1021/acs.jpcc.8b06681.

Tabulated Gaussian fit parameters for the catalase crystal, cryo-TEM analysis of the same crystals, and details of the synthesis and characterization of the peptoid nanosheets (PDF)

■ AUTHOR INFORMATION

Corresponding Author

*E-mail: scott.lea@pnnl.gov.

ORCID

Brian T. O'Callahan: 0000-0001-9835-3207
Kevin T. Crampton: 0000-0002-1258-7895
Markus B. Raschke: 0000-0003-2822-851X
Patrick Z. El-Khoury: 0000-0002-6032-9006

Notes

The authors declare no competing financial interest.

■ ACKNOWLEDGMENTS

A.S.L., B.T.O, K.T.C., M.B.R, and P.Z.E. are supported by the Department of Energy (DOE), Office of Science Biological and Environmental Research (BER) Bioimaging Technology Project no. 69212. I.V.N. and J.E.E. provided the catalase sample and cryo-TEM analysis and acknowledge support from DOE-BER Bioimaging Technology Project no. 66382. T.J. and C.-L.C provided the peptoid sample and acknowledge support from DOE Office of Basic Energy Sciences, and Biomolecular Materials Program at PNNL. This work was performed in the Environmental and Molecular Sciences Laboratory (EMSL), a DOE Office of Science User Facility sponsored by BER and located at Pacific Northwest National Laboratory (PNNL). PNNL is operated by Battelle Memorial Institute for the DOE under Contract no. DE-AC05-76RL1830.

■ REFERENCES

(1) Jones, S.; Thornton, J. M. Principles of Protein-protein Interactions. *Proc. Natl. Acad. Sci. U. S. A.* **1996**, *93*, 13−20.

(2) Surewicz, W. K.; Mantsch, H. H.; Chapman, D. Determination of Protein Secondary Structure by Fourier Transform Infrared Spectroscopy: A Critical Assessment. *Biochemistry* **1993**, *32*, 389−394.

(3) Ilari, A.; Savino, C. Protein Structure Determination by X-Ray Crystallography. In *Bioinformatics: Data, Sequence Analysis and Evolution*; Keith, J. M., Ed.; Humana Press: Totowa, NJ, 2008; pp 63−87.

(4) Chapman, H. N.; Fromme, P.; Barty, A.; White, T. A.; Kirian, R. A.; Aquila, A.; Hunter, M. S.; Schulz, J.; DePonte, D. P.; Weierstall, U.; et al. Femtosecond X-ray Protein Nanocrystallography. *Nature* **2011**, *470*, 73−77.

(5) Paulite, M.; Fakhraai, Z.; Li, I. T. S.; Gunari, N.; Tanur, A. E.; Walker, G. C. Imaging Secondary Structure of Individual Amyloid Fibrils of a β2-Microglobulin Fragment Using Near-Field Infrared Spectroscopy. *J. Am. Chem. Soc.* **2011**, *133*, 7376−7383.

(6) Berweger, S.; Nguyen, D. M.; Muller, E. A.; Bechtel, H. A.; Perkins, T. T.; Raschke, M. B. Nano-Chemical Infrared Imaging of Membrane Proteins in Lipid Bilayers. *J. Am. Chem. Soc.* **2013**, *135*, 18292−18295.

(7) Amenabar, I.; Poly, S.; Nuansing, W.; Hubrich, E. H.; Govyadinov, A. A.; Huth, F.; Krutokhvostov, R.; Zhang, L.; Knez, M.; Heberle, J.; et al. Structural Analysis and Mapping of Individual Protein Complexes by Infrared Nanospectroscopy. *Nat. Commun.* **2013**, *4*, 2890.

(8) Bechtel, H. A.; Muller, E. A.; Olmon, R. L.; Martin, M. C.; Raschke, M. B. Ultrabroadband Infrared Nanospectroscopic Imaging. *Proc. Natl. Acad. Sci. U. S. A.* **2014**, *111*, 7191−7196.

(9) Muller, E. A.; Pollard, B.; Raschke, M. B. Infrared Chemical Nano-Imaging: Accessing Structure, Coupling, and Dynamics on Molecular Length Scales. *J. Phys. Chem. Lett.* **2015**, *6*, 1275−1284.

(10) Barth, A. Infrared Spectroscopy of Proteins. *Biochim. Biophys. Acta, Bioenerg.* **2007**, *1767*, 1073−1101.

(11) Atkin, J. M.; Sass, P. M.; Teichen, P. E.; Eaves, J. D.; Raschke, M. B. Nanoscale Probing of Dynamics in Local Molecular Environments. *J. Phys. Chem. Lett.* **2015**, *6*, 4616−4621.

(12) Pollard, B.; Muller, E. A.; Hinrichs, K.; Raschke, M. B. Vibrational Nano-spectroscopic Imaging Correlating Structure with Intermolecular Coupling and Dynamics. *Nat. Commun.* **2014**, *5*, 3587.

(13) Xu, X. G.; Raschke, M. B. Near-Field Infrared Vibrational Dynamics and Tip-Enhanced Decoherence. *Nano Lett.* **2013**, *13*, 1588−1595.

(14) Taubner, T.; Hillenbrand, R.; Keilmann, F. Performance of Visible and Mid-infrared Scattering-type Near-field Optical Microscopes. *J. Microsc. (Oxford, U. K.)* **2003**, *210*, 311−314.

(15) Jin, H.; Jiao, F.; Daily, M. D.; Chen, Y.; Yan, F.; Ding, Y.-H.; Zhang, X.; Robertson, E. J.; Baer, M. D.; Chen, C.-L. Highly Stable and Self-repairing Membrane-mimetic 2D Nanomaterials Assembled from Lipid-like Peptoids. *Nat. Commun.* **2016**, *7*, 12252.

(16) Aizpurua, J.; Taubner, T.; García de Abajo, F. J.; Brehm, M.; Hillenbrand, R. Substrate-enhanced Infrared Near-field Spectroscopy. *Opt. Express* **2008**, *16*, 1529−1545.

(17) Nannenga, B. L.; Shi, D.; Hattne, J.; Reyes, F. E.; Gonen, T. Structure of Catalase Determined by MicroED. *eLife* **2014**, *3*, No. e03600, DOI: 10.7554/eLife.03600.

(18) Raschke, M. B.; Molina, L.; Elsaesser, T.; Kim, D. H.; Knoll, W.; Hinrichs, K. Apertureless Near-Field Vibrational Imaging of Block-Copolymer Nanostructures with Ultrahigh Spatial Resolution. *ChemPhysChem* **2005**, *6*, 2197−2203.

(19) Mukherjee, P.; Krummel, A. T.; Fulmer, E. C.; Kass, I.; Arkin, I. T.; Zanni, M. T. Site-specific Vibrational Dynamics of the CD3zeta Membrane Peptide using Heterodyned Two-dimensional Infrared Photon Echo Spectroscopy. *J. Chem. Phys.* **2004**, *120*, 10215−24.

(20) Londergan, C. H.; Wang, J.; Axelsen, P. H.; Hochstrasser, R. M. Two-Dimensional Infrared Spectroscopy Displays Signatures of Structural Ordering in Peptide Aggregates. *Biophys. J.* **2006**, *90*, 4672−4685.

(21) Jiao, F.; Chen, Y.; Jin, H.; He, P.; Chen, C.-L.; De Yoreo, J. J. Self-Repair and Patterning of 2D Membrane-like Peptoid Materials. *Adv. Funct. Mater.* **2016**, *26*, 8960−8967.

(22) Levinson, N. M.; Fried, S. D.; Boxer, S. G. Solvent-Induced Infrared Frequency Shifts in Aromatic Nitriles Are Quantitatively Described by the Vibrational Stark Effect. *J. Phys. Chem. B* **2012**, *116*, 10470−10476.

(23) Hao, F.; Jing, M.; Zhao, X.; Liu, R. Spectroscopy, Calorimetry and Molecular Simulation Studies on the Interaction of Catalase with Copper Ion. *J. Photochem. Photobiol., B* **2015**, *143*, 100−106.

DOI: 10.1021/acs.jpcc.8b06681
J. Phys. Chem. C 2018, 122, 24891−24895